Relationship of intracloud lightning radiofrequency power to lightning storm height, as observed by the FORTE satellite

Abram R. Jacobson

Space and Atmospheric Sciences Group, Los Alamos National Laboratory, Los Alamos, New Mexico, USA

Received 17 September 2002; revised 4 November 2002; accepted 9 January 2003; published 3 April 2003.

[1] Prior studies have noted a strongly nonlinear enhancement of lightning flash rates with increasing cloud height. Here we report a related observation, of a tendency for increasing intracloud-discharge radiofrequency-emission power for increased height of the electrified cloud. The FORTE satellite's radio-frequency-receiver payload has performed extensive recordings of electromagnetic emissions of lightning discharges. The most commonly occurring such emission arises from intracloud electrical breakdown and is usually recognizable by a pulse followed by a delayed echo from the ground reflection. We have used other systems of lightning monitors to provide source locations for an extended data set of FORTE intracloud-discharge signals. The interpulse separation within each pulse pair yields the discharge height above the reflective ground. The storm in which the pulse occurs usually provides many (at least 50) recorded events. From the pattern of these events' heights, we can usually infer a capping height, which serves as an upper bound on the lightning discharge heights for that storm. We find that there is a strong statistical increase of effective radiated power of intracloud discharges, for increasing capping height of the parent storm. Thus a future satellite-based lightning monitor that triggers on only the most intense radiofrequency emissions will be strongly selective for electrified storms with very deep vertical development. Such storms are also indicated in severe convective weather. *INDEX TERMS:* 3314 Meteorology and Atmospheric Dynamics: Convective processes; 3304 Meteorology and Atmospheric Dynamics: Atmospheric electricity; 3324 Meteorology and Atmospheric Dynamics: Lightning; 3329 Meteorology and Atmospheric Dynamics: Mesoscale meteorology; 3360 Meteorology and Atmospheric Dynamics: Remote sensing; *KEYWORDS:* lightning, severe storms, thunderstorms, storm electrification, remote sensing

Citation: Jacobson, A. R., Relationship of intracloud lightning radiofrequency power to lightning storm height, as observed by the FORTE satellite, *J. Geophys. Res.*, *108*(D7), 4204, doi:10.1029/2002JD002956, 2003.

1. Introduction

[2] While lightning is a dramatic natural phenomenon in itself, it is also attracting growing interest as a remote-sensing marker of tropospheric deep convection and severe weather. Space-based remote sensing offers, in principle, unhindered access to the entire atmosphere, including the southern oceans and uninhabited areas. Lightning can be monitored from space by satellite-based detection of both optical [e.g., *Boccippio et al.*, 2000a; *Christian et al.*, 1999a, 1999b; *Kirkland et al.*, 2001; *Light et al.*, 2001a; *Suszcynsky et al.*, 2001] and radio-frequency (RF) lightning signatures [e.g., *Jacobson et al.*, 1999, 2000; *Light and Jacobson*, 2002; *Shao and Jacobson*, 2002].

[3] In order for lightning's remote-sensing utility to be fully realized in providing useful information in meteorology, hydrology, and climate studies, two areas of effort are needed: (a) better instrumentation, or at least reliable instrumentation on satellite constellations offering more synoptic coverage, and (b) appropriate data-exploitation strategies. Space-borne instrumentation initiatives are currently being pursued, including both geostationary-satellite-based optical imagers [*Christian et al.*, 1989] and Global Positioning Satellite (GPS)-based RF detectors [*Suszcynsky et al.*, 2000a]. Either, and possibly both of those systems in parallel, could eventually provide quasi-real-time, synoptic lightning data over the entire tropical and midlatitude regions. Appropriate data exploitation must be based on the unique characteristics of each type of sensor, and on how those characteristics serve as indicators of meteorological conditions or trends. It would be especially unfortunate if the remote-sensing signatures that are visible from space were merely indicating idiosyncratic and insignificant meteorological conditions. This paper addresses the issue for RF remote sensing and concludes that RF observations are likely to highlight the most intense, deeply developed atmospheric convection.

[4] Satellite RF lightning monitoring is able to measure the lightning discharge height, not just the horizontal position (latitude, longitude). This ability is unique to the RF approach: The optical signature of lightning seen from space is a transient cloud top brightening, regardless of where (in height) the lightning occurs in the atmospheric

0148-0227/03/2002JD002956$09.00

column underneath the cloud top. Optical photons are elastically Mie-scattered tens to hundreds of times, in what is effectively a diffusion process through the cloud [*Koshak et al.*, 1994; *Light et al.*, 2001b] before emerging from the cloud top. By contrast, RF propagates through clouds with neither scattering nor attenuation. A future GPS-based RF monitor would use differential-time-of-arrival (DTOA) methods to retrieve not only the discharge plan location (longitude, latitude) but also the discharge altitude [*Suszcynsky et al.*, 2000a].

[5] This paper reports on the behavior of lightning discharge heights as revealed by data from the FORTE satellite [*Jacobson et al.*, 1999]. The goal is to clarify how best to utilize these height data, and we illustrate this via correlation with another RF observable, the radiated power at the source. We show that there is a statistical correlation between RF radiated power and the capping height (i.e., the top height of RF discharges) of the storm.

[6] The paper is organized as follows: Section 2 (Background) reviews why discharge height is expected to be a valuable and significant remote-sensing observable. Section 3 (methodology) introduces the basic data characteristics and analysis tools that are used to derive lightning discharge heights with FORTE. Section 4 (Results and discussion) shows the raw results and discusses how they can be better illuminated by consideration of the capping height of the storm containing any particular discharge, rather than the proper height of each discharge.

2. Background

[7] Why is thunderstorm height important to monitor? It is now widely accepted that thunderstorm electrification usually requires collisions between graupel (or hail) and ice crystals in the presence of supercooled water (see, e.g, the review by *Baker et al.* [1999]). *Blyth et al.* [2001] have shown on the basis of scaling relationships that a thundercloud's lightning flash rate (f) is expected to be ''proportional to the product of the downward flux of solid precipitation (i.e, graupel and hail) through the body of the thundercloud and the upward flux of ice crystals into the anvil.'' In a useful review on the electrification of severe storms, *Williams* [2001] (subsequently W2001) shows that having a sustained presence of mixed-phase-hydrometeors together in the same region requires the cloud to have deep vertical development: The cloud must extend upward to the −40 Celsius isotherm or thereabouts, and must implicitly contain an intense core updraft. The latter can lead to tropopause overshoot (see in particular Figure 13.14 of W2001) and thus to water ice insertion into the normally dry stratosphere.

[8] There is a wide and emerging consensus based on observations as well, that the stronger the thundercloud convection, and the higher the thundercloud development, then the more vigorous is the lightning (all other things being equal.) This is reviewed in W2001, and only a few pertinent recent developments will be cited here.

[9] The most common observable of a thunderstorm's lightning vigor is the flash rate of lightning in the storm. Several ground-based lightning studies, reviewed by W2001, indicate that the flash rate f of a thundercloud is strongly correlated with the radar cloud top height h (see in particular Figures 13.6 and 13.7 in W2001). Those data suggest a dependence $f \sim h^5$ over continental settings, although the scatter is considerable. More recent studies with the TRMM satellite, in which the TRMM-borne precipitation radar (PR) characterizes the cloud top height, and in which the TRMM-borne Lightning Imaging Sensor (LIS) determines the colocated flash rate, yield an improved statistical test of the power law hypothesis [*Ushio et al.*, 2001]. The scatter is enormous, but still, there is a statistical tendency for increasing cloud height to lead to increasing flash rate. Fitting a power law model to height-binned averages of the flash rate, *Ushio et al.* find power law exponents over land in the range 4 to 5. The data over ocean is sparser and hence yields statistically less significant results. There is also some indication of dependence on season. Overall, the results of *Ushio et al.* confirm the general trend of the earlier studies reviewed in W2001. However, the scatter of the data seen by TRMM shows that the nonlinear dependence, of flash rate on cloud depth, is a statistical but not an instantaneous relationship.

[10] Another indicator of storm height is the scattering of upwelling microwave, for example, ∼37 GHz and ∼85-GHz, radiation due to ice crystals in the upper portion of clouds. This is routinely measured aboard TRMM by the TRMM Microwave Imager (TMI) in a wide (760-km) swath aligned within the LIS image swath [*Kummerow et al.*, 1998]. The TMI is similar to the Special Sensor Microwave Imager (SSM/I) carried by the DMSP satellites. The degree of scattering is greater, the more highly glaciated the cloud. Insofar as this is a similar physical circumstance as produces lightning [*Baker et al.*, 1999; *Blyth et al.*, 2001], the ice-crystal scattering and subsequent depression of microwave apparent brightness temperature is expected to correlate with lightning vigor. Focusing on mesoscale convective systems (MCSs), *Toracinta and Zipser* [2001] compared regional/seasonal climatologies of SSM/I 85-GHz scattering signatures with OTD lightning flash rates. They found close positive correlation these two variables' climatologies in all continental regions during all seasons, particularly for the most intense MCS clusters.

[11] *Boccippio et al.* [2000b] have further studied OTD and LIS flash-rate geographical distributions and clarified the land/sea contrast (a factor of ∼10 in gross flash rate, favoring land) seen by those instruments [see also *Boccippio*, 2002, Figure 1]. They find that the land/sea contrast per storm is only a factor of ∼2, but that marine storms possessing lightning-prone characteristics have wider geographical separation and less frequent temporal occurrence.

[12] A subsequent study [*Toracinta et al.*, 2002] with the TMI, PR, and LIS instruments aboard TRMM addresses the issue of whether all three variables, namely ice-scattering signatures, precipitation-radar cross-sections, and lightning flash rates (respectively) are correlated for individual storms, not just statistically. Their study shows that the three variables are correlated in individual storms, albeit with some scatter. For example, results on continental tropical South America and Africa regions both show that 40-dBz PR heights are confined to <9 km for storms without LIS lightning, while 40-dBz PR heights extend to <15 km for storms with LIS lightning [see *Toracinta et al.*, 2002, Figure 9]. Similarly, these same storms show 37-GHz apparent brightness temperatures down only to 250 K for storms without LIS lightning, while 37-GHz apparent

brightness temperatures extend down to 150 K for storms with LIS lightning [see *Toracinta et al.*, 2002, Figure 8]. The same study verifies the correspondence in reverse also: Continental storms with 37-GHz apparent brightness temperatures below 240 K essentially all have LIS-detected lightning, while less than 30% of continental storms with 37-GHz apparent brightness temperatures above 280 K have LIS-detected lightning. Similarly, continental storms with PR 30-dBz heights above 11 km essentially all have LIS-detected lightning, while fewer than 30% of continental storms with PR 30-dBz heights below 7 km have LIS-detected lightning [see *Toracinta et al.*, 2002, Figure 10].

[13] This paper will report on initial observations of an analogous relationship between storm height and lightning vigor, but with the lightning vigor being sensed by RF emissions. Given that the FORTE satellite carries neither a radar (like the TRMM PR) nor a microwave imager (like the TRMM TMI), our inference of storm height cannot derive from such nonlightning data, at least not on such data provided by FORTE itself. Instead, our inference is based on the distribution of lightning discharge heights for each storm. In this present paper, we find that the RF effective radiated power (ERP, or isotropic peak power radiated from the source in the receiver bandwidth) is a significant statistical correlate of storm height as inferred from contemporaneous FORTE RF data.

[14] In the future we will report RF ''flash rate'' observed by FORTE, but we are not yet in a position to correct for observational biases (background noise, storm-satellite distance, and instantaneous trigger thresholds). Without such a correction, the inter-storm comparisons of flash rates would be biased (see, e.g., the correction for LDAR detection-efficiency biases given by *Boccippio et al.* [2000c, 2000d]).

3. Methodology

3.1. RF Payload Characteristics

[15] The FORTE satellite is in a circular orbit at altitude $\sim$800 km and inclination 70°. The radio subsystem aboard FORTE receives, digitizes, stores, and downlinks discrete records of very-high-frequency (VHF) lightning time series waveforms of the RF electric field, E. The radio-frequency receiver whose data are used in much of this study comprises dual, simultaneous 50-Megasample-per-second passbands that are simultaneously digitized, each analog-filtered to 22-MHz bandwidth [*Jacobson et al.*, 1999]. In the data to follow, we always operated the RF payload with at least one of the 22-MHz-bandwidth channels placed in the range 26–48 MHz, with a nominal 38-MHz center (''low band''). During some of the study, the other 22-MHz-bandwidth channel was tuned to ''high band'' (118–140 MHz), with a nominal 130-MHz center. Otherwise, the other 22-MHz channel was tuned to low band also, so that both channels were on low-band, but on orthogonal antennas. The trigger for both channels was common and was always derived from low band. The performance of the FORTE RF payload, plus some of the initial characteristics of the lightning observations, has been described in detail elsewhere [*Jacobson et al.*, 1999], so only the most pertinent information is repeated here.

[16] FORTE uses a multichannel-coincidence trigger that allows triggering on very weak lightning emissions. There are eight ''trigger subbands'' in each 22-MHz-wide receiver channel. Each 1-MHz-wide trigger subband has a noise-compensation option, so that the trigger threshhold is set either in absolute level or as dB above a low-pass-filtered noise level in that 1-MHz subband, that is, as a ''noise-riding threshold.'' In this way the trigger system can in practice trigger on lightning signatures that would otherwise be overwhelmed by anthropogenic radio carriers appearing in the overall receiver passband. In the data used here, we use noise-riding-threshhold triggering and require five (out of eight) 1-MHz subbands to trigger in approximate coincidence. We typically require the signal to rise at least 14–20 dB (depending on the program and the intended class of lightning signals) above the noise background in each 1-MHz subband contributor to the ''5-out-of-8'' logical-OR condition. These contributing channels must arrive within a coincidence time of 162 μs of each other. This coincidence window allows for arrival of different frequencies from the same event, in the presence of ionospheric dispersion of the pulse. (''Ionospheric dispersion'' is the effect of the ionospheric plasma's imposing a group delay on the rf pulse, with the delay varying roughly as $1/f^2$.) The exceptional peformance of the multichannel-coincidence trigger has allowed FORTE to trigger on, and to record, lightning VHF emissions with ERP (in the passband 26–48 MHz) from high levels ($\sim 10^6$ W) down to very weak levels ($\sim 10^3$ W) [*Jacobson et al.*, 2000]. In all uses of the term ''ERP'' to follow, it is to be understood that we refer to peak power integrated over the passband 26–48 MHz, the FORTE low band.

[17] The ionospheric $1/f^2$ dispersion causes the lowest frequencies to arrive latest, as in a ''chirp.'' For this reason the VHF signals, which have been transmitted through the ionosphere, are referred to as ''chirped'' signals. Similarly, the signal-processing step of removing the dispersion is called ''dechirping.'' We perform dechirping on all archived VHF signals from FORTE. Dechirping is performed prior to estimation of the ERP. Without dechirping, the ERP estimate would be artificially low, because the arrival of energy across the passband would be time-dispersed.

[18] Both 22-MHz-bandwidth channels are connected to different linear polarizations of a two-polarization log-periodic antenna. The antenna is mounted on a boom toward the satellite nadir, usually within a few degrees or less of true pointing. The antenna is designed to place an approximate minimum (throughout the VHF spectrum) on the limb of the Earth as seen from FORTE, and a lobe maximum at nadir. The limb is a circle of arc-diameter 6,400 km on the surface of the Earth. The performance of this antenna system is described in detail elsewhere [*Jacobson and Shao*, 2002b; *Massey et al.*, 1998; *Shao and Jacobson*, 2001, 2002].

[19] The Data Acquisition System (DAS) contains enough memory for up to 0.8 seconds s (cumulative) of 12-bit data simultaneously from the two 22-MHz channels. Each record is triggered (see above) and has adjustable pre/posttrigger ratio for the record-trigger alignment. We typically use 400-μs records that contain 100 μs of pretrigger samples and 300 μs of posttrigger samples.

[20] The DAS is capable of beginning a new record 162 μs after the end of the previous record, so that FORTE records can effectively be strung-together to form a quasi-continuous registation of VHF signatures arriving one-upon-the-other within a flash. We find in practice that the

registration of records is not impeded by the necessary DAS dead time between records, but rather is spaced wider apart by the natural cadence of the emission process itself.

[21] The configuration described above was followed between launch (August 1997) and December 1999. During this ~28-month campaign, FORTE gathered over 3-million data records, the vast majority of which were due to VHF emissions from lightning.

3.2. FORTE RF Data Characteristics

[22] Most FORTE records derive from intracloud (IC) lightning discharges. This is not surprising, in view of the overall dominance of IC flashes (as opposed to ground flashes) [*Boccippio et al.*, 2001] and in view of the increase of IC dominance as storm intensity increases [see, e.g., W2001, Figure 13.8]. Sometimes FORTE records IC radio emissions that are wide in time, e.g., >10 μs, arising from recoil-streamer activity (as shown in Figure 2 of *Light et al.*, 2001a). These wide IC pulses will be excluded from consideration in this study, as their width usually interferes with the "echo" that follows the main emission, typically delayed by >10 μs: An IC pulse received by FORTE is accompanied by a delayed, second pulse due to the ground-reflection echo. Figure 1a shows the emitter ("e"), the reflective ground, and the signal paths for both the direct and ground-reflected signals. Figure 1b shows the geometry of the rays near the ground. The ground-reflected echo signal travels an additive distance equal to p−q, relative to the direct signal. This additive distance, divided by the speed of light, gives the time lag of the second pulse relative to the first pulse. Conversion of the measured time lag to a discharge height (=*a* Figure 1b) requires knowledge of the satellite elevation angle β. This angle is derivable if we know the lightning horizontal location (see below).

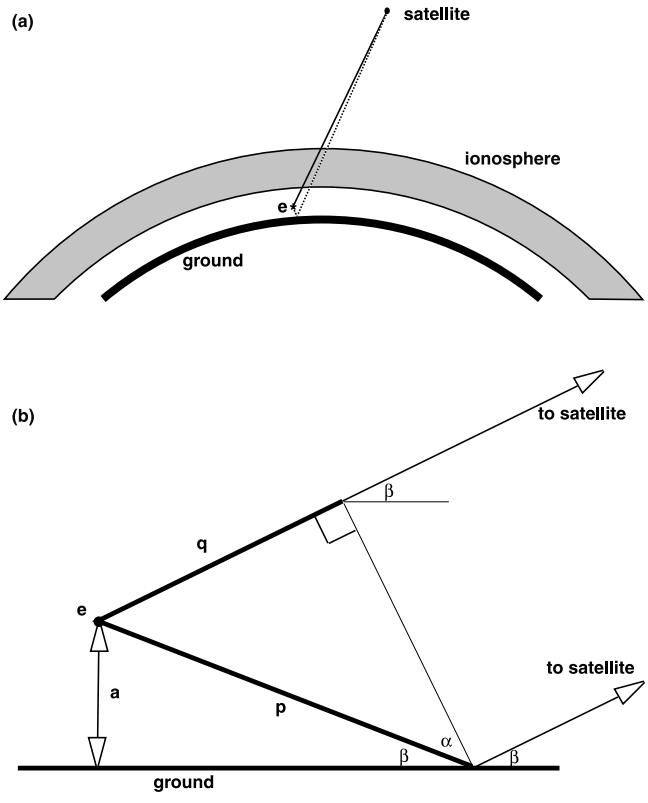

Figure 1. (a) Schematic of emitter ("e"), ground surface, ionosphere, and satellite. Direct path from the emitter to the satellite is shown as a solid line. Ground-reflection indirect path is shown as a dotted line. (b) Close-in view of the reflection geometry (see text). Emitter "e" is at height "a" above the reflective ground. Satellite elevation angle is β.

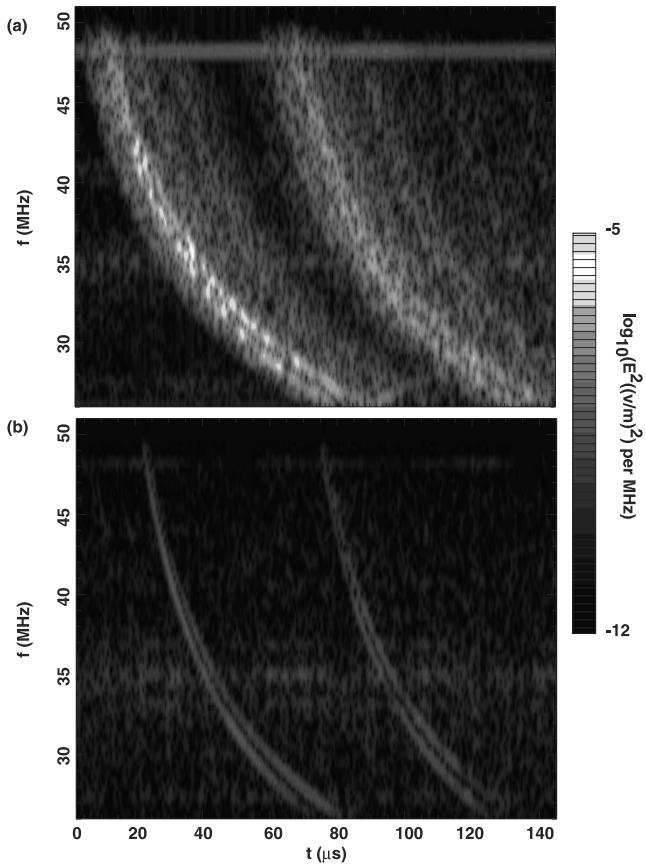

Figure 2. Spectrograms of (a) strong intracloud pulse, and (b) polarized/coherent intracloud pulse. The ground echo is seen at a delay of ~50–60 μs relative to the main pulse in each case. The spectrogram is computed with a sliding short-period Fourier transform having ~1-μs width. Gray-scale key is shown at right.

[23] Figure 2 shows examples of FORTE-recorded intracloud pulses, each followed by the delayed ground-reflection echo (about 50–60 μs later). The data are shown as spectral density of the received electric field, versus time (on the horizontal axis) and frequency (on the vertical axis). The spectral density in each column is estimated in a short-time windowed Fourier transform. The pulse itself, and its echo, are each split due to geomagnetic birefringence in the ionosphere [*Jacobson and Shao*, 2001; *Massey et al.*, 1998]. The gray scale codes the logarithm (base 10) of the spectral density. The two examples in Figure 1 show opposite, contrasting types in the variety of IC pulses usually recorded by FORTE. Figure 1a shows an intense pulse having relatively wide pulse-shape (3–5 μs), unpolarized radiation, random intrapulse fading (amplitude variations), and an extended (several additional μs) pulse continuation at much lower power than the main pulse [*Jacobson and*

Light, 2003]. Figure 2b shows a weaker IC pulse, which has a narrower (<1 μs) pulse-shape, coherent nonfading pulse structure, and linearly polarized radiation [*Jacobson and Light*, 2003]. The weak pulse in Figure 2b could not have been triggered upon with a simple wideband-amplitude trigger. Instead, weak pulses of this sort can be triggered upon only with a multichannel-coincidence system.

[24] The pulse intensities in the two examples in Figure 2 differ by three orders-of-magnitude. The intense pulses (Figure 2a) can be seen by FORTE anywhere they occur. The faint pulses (Figure 2b), on the other hand, can be seen only in radio-quiet parts of the Earth. The majority of radio noise seen by FORTE is from anthropogenic (communications, radar, and industrial) radio emissions. These emissions are very strong over North America, Europe, and East Asia. By contrast, anthropogenic radio emissions are relatively weak over the southern hemisphere and in particular over the southern oceans. FORTE's noise-riding-threshold trigger system (see section 3.1 above) adjusts to ambient radio noise and in effect applies an absolute trigger threshold that is higher in noisy regions and lower in quiet regions. As a result, the ambient radio noise forces the RF-intensity spectrum for lightning RF signals to be truncated at different intensities, depending on the region over which the satellite is located at any instant.

[25] This is illustrated in Figure 3, which shows histograms of root-mean squared peak pulsed electric field (V/m) at the satellite for two selected subdistributions of the ~3.1-million FORTE archived lightning events recorded from 1997–1999. We use electric field rather than intensity, in order to compress the horizontal range. The selection criteria require that the pulse signal-to-noise ratio (snr) be >3, that the second pulse meet further snr criteria [*Jacobson et al.*, 1999], and that the satellite be in a geographical zone noted next to each curve. The lighter curve is for subsatellite points anywhere in the southern hemisphere. The heavier curve is for twice the distribution within North America (i.e., FORTE in a box given by $-120 <$ longitude < -60 degrees, and $25 <$ latitude < 55 degrees). These subdistributions contain 241,315 and 45,584 IC pulse events respectively. The higher-power tail of these distributions is dominated by IC pulses similar to the pulse in Figure 2a, while the low-power peak is dominated by IC pulses similar to the pulse in Figure 2b. Of the two curves, the Southern Hemisphere distribution contains a larger fraction of weak pulses of the type shown in Figure 2b, because of that region's relatively low background noise.

[26] Each curve in Figure 3 shows a similar slope to the right (i.e., at the higher-field side) of the peak of the distribution. This is because detection of these high-field pulses occurs at a rate unaffected by the trigger threshold, which is well below these pulses. Instead, the high-field tail of both distributions reflects the intrinsic amplitude spectrum of the RF pulse fields from lightning, seen by a platform at 800-km altitude. Further to the left in each distribution, however, the two curves differ markedly. The southern-hemisphere distribution peaks at a field amplitude that is several-fold weaker than is the field amplitude at which the North America distribution peaks. In other words, the two pulse-field-amplitude distributions are truncated at different effective field strengths, depending on satellite position vis a vis the geographical distribution of background radio noise. Around and to the left of each truncation point, the distribution is heavily biased by the noise. To the right of each truncation point, the distribution is basically unaffected by the noise.

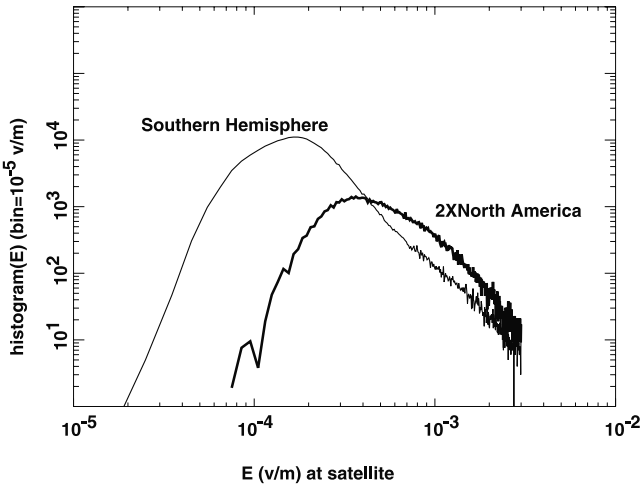

Figure 3. Histogram of the root-mean square peak electric field amplitude at the satellite, in a 1-μs average near the pulse peak. The binwidth is 10^{-5} v/m. The lighter curve is for the entire southern hemisphere, while the heavier curve is twice the histogram from a rectangle centered on the United States and given by $-120 <$ longitude < -60 degrees, and $25 <$ latitude < 55 degrees. These subdistributions contain 241,315 and 45,584 IC pulse events, respectively.

[27] FORTE can monitor the incidence of very strong pulses (like the pulse in Figure 2a) in a relatively unbiased manner between different geographical regions. However, FORTE's recorded incidence of weak pulses (like the pulse in Figure 2b) is subject to strong biases when it comes to comparing different geographical regions. Until this bias can be properly compensated, it is premature to compare overall "flash rates" between geographical regions based on FORTE RF data. We note that this compensation will be more complicated than was the case with LDAR [*Boccippio et al.*, 2000c, 2000d], because the satellite moves continuously over the globe and therefore experiences time-evolving noise backgrounds.

3.3. Inference of RF-Discharge Horizontal Location

[28] As is obvious from Figure 1, the height of IC discharges can be inferred from FORTE pulse-separation data if the horizontal location of the discharge is known. Another benefit of knowing the horizontal location is that the received pulse amplitude can be converted to an ERP at the source, which is more physically relevant. FORTE by itself cannot directly measure the location of sources of received RF pulses. This is not a limitation on satellite constellations capable of differential-time-of-arrival (DTOA) source-location. However, FORTE is a single satellite and therefore cannot rely on DTOA techniques. In order to circumvent this, FORTE RF signals' arrival times have been compared with several independent lightning location systems. FORTE has relied in this procedure on correlation with data from the National Lightning Detection Network (see the description of methods and results given by *Jacobson et al.* [2000]),

from the United Kingdom Meteorological Office long-range lightning location array (for a description of the lightning location array but not of the correlation with FORTE, see, e.g., *Lee* [1986]), from the Los Alamos Sferic-Waveform Array centered on Florida [*Smith et al.*, 2001], and from the CCD-imager Lightning Location System (LLS) on FORTE itself [*Light et al.*, 2001a; *Suszcynsky et al.*, 2000b]. Cumulatively these sources of lightning location information allow us to state, with considerable (>95%) certainty, the longitude and latitude of the discharges providing over 50,000 FORTE RF records.

[29] Of the FORTE RF pulses whose source locations have been inferred by correlation with other systems, many of these pulses can be clearly associated with other FORTE RF pulses, either in the same flash or in at least the same storm. It is then possible for the clearly associated pulses to "borrow" the source location of a pulse whose source is known. In this manner we can expand the set of events whose source location is known and whose data can then yield both an IC-discharge height and an at-source ERP. This borrowing procedure has been described in detail elsewhere [*Jacobson and Shao*, 2002b; *Tierney et al.*, 2001] but will be briefly illustrated here for clarity.

[30] During a FORTE pass within view of a storm or within view of a region containing more than one storm, the path-integrated ionospheric density, or total electron content (TEC), can serve as a discriminant between signals from different storms. The TEC is routinely retrieved for each RF signal [*Jacobson et al.*, 1999] recorded by FORTE. The TEC is roughly proportional to the distance through the ionosphere of the source-to-FORTE line-of-sight. Thus, storms more distant from FORTE tend to have higher TEC, and storms closer to FORTE tend to have lower TEC, in their recorded RF signals. Also, for a given storm, the TEC varies smoothly as FORTE's position relative to the storm evolves (i.e., as FORTE passes from horizon to horizon.) When FORTE is closest to the storm ("culmination"), the ionospheric path is shortest, and the TEC is least. When FORTE is further from the storm, that is, when FORTE is lower in the sky seen from the storm, the ionospheric path is longer, and the TEC is higher. These systematics can be understood with the schematic of Figure 1a.

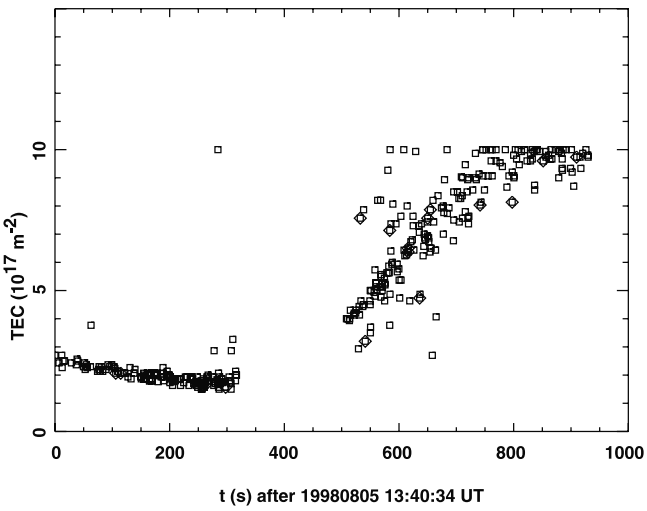

Figure 4. TEC versus time during a FORTE pass within view of lightning emissions. (The saturation of TEC at the upper-right is an artifact of the algorithm's imposed maximum TEC of 10×10^{17} m^{-2}.) There is an observing gap (t = 300 to t = 500 s) during which FORTE's RF trigger is not armed.

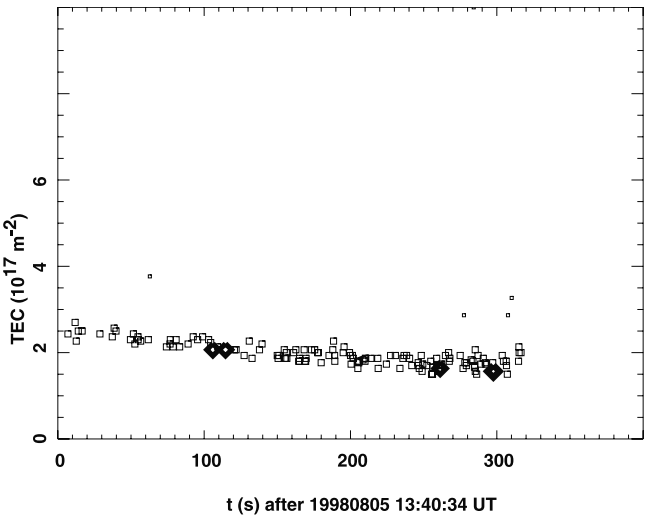

Figure 5. TEC versus time during the first 400 s of Figure 4. Small square symbols are for rejected events. Medium square symbols are for accepted events. Large, dark diamond symbols are for the accepted events that have prior location data from other sources (in this case, NLDN).

[31] Figure 4 shows TEC versus time during a FORTE pass within view of lightning emissions. (The saturation of TEC at the upper-right of Figure 4 is an artifact of the algorithm's imposed maximum TEC of 10×10^{17} m^{-2}.) There is an observing gap (t = 300 to t = 500 s) during which FORTE's RF trigger is not armed. Culmination occurs late in the first observing interval (t = 200 to 300 s). There is one dominant contributing storm, although there are several events whose TEC values clearly indicate that those events' sources are from differently located storms. Figure 4 shows a total of 358 recorded events, from which we want to select only those events which clearly derive from the dominant contributing storm. To do this we perform an interactive procedure which first limits attention to a useable portion of the pass that contains at least three events whose source locations are already known (by correlation to other systems as described above). In the case of Figure 4 we limit further attention to the first observing time, prior to the data gap. We then fit a smooth polynomial to the TEC-versus-time trend of the dominant storm's TEC values, and finally impose a filter to reject outlier events whose TEC is not within a band of TEC residuals closely centered on the smooth polynomial. The result in this case is shown in Figure 5. The small square symbols are for rejected events. The medium square symbols are for accepted events. The large, dark diamond symbols are for the accepted events that have prior location data from other sources (in this case, NLDN). There are four such located sources, so that the selected data in Figure 5 meet the criterion of there being at least three located sources in order for location-borrowing to proceed.

[32] In Figure 5 there are 140 accepted events including the four whose locations are already known. That means

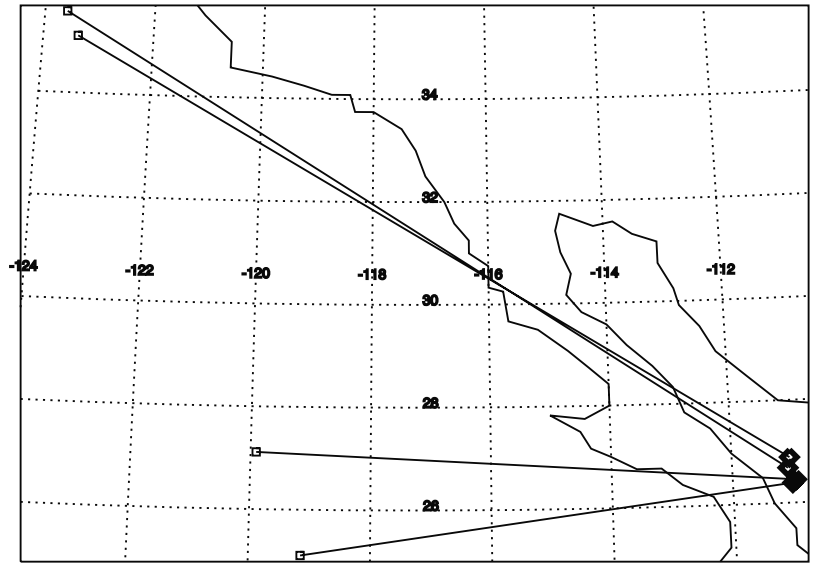

Figure 6. Map NLDN-furnished lightning positions (large diamonds) during the portion of orbit corresponding to Figure 5. Each lightning position is connected to the subsatellite point of FORTE (small squares) at the time of that lightning event's observation.

that we will be able to let the 136 events borrow the location indicated by the 4 events, provided that the consensus location of those four events is consistent. Figure 6 shows a map of the four known locations (heavy diamonds, in the Sea of Cortez) as well as the four corresponding FORTE positions (light squares, over the Pacific Ocean.) We calculate the average longitude and average latitude of the lightning events, and then require that each of the four source locations lie within 300 km radial distance from the average location. This criterion is satisfied by the present example, resulting in the "gain" of 136 FORTE event source locations borrowed as the average of the four known locations.

[33] The 140 selected events from Figure 5 contain mostly IC pulses. Figure 7a shows the interpulse separation for these IC events as a function of time during the satellite pass. The overall upward trend is due to the approach to culmination. The interpulse separation is expected to vary from a low value, when the satellite is on the horizon, to a higher value, when the satellite culminates, or reaches closes approach to the storm [*Jacobson et al.*, 1999]. Figure 7b shows the resultant discharge heights above the ground, as inferred using both the interpulse separation and the relative location of the storm and the satellite [*Jacobson et al.*, 1999]. Each inferred height in Figure 7b utilized the instantaneous satellite position as it moves S/SE during this pass. Most of the discharges in this storm occur at heights between 9 and 15 km. Most of the discharges in this storm occur at heights between 9 and 15 km. The height is the height above the local ground. Most of the observed lightning occurs at either sea level or very low (<0.2 km) altitude, so the discrepancy between height and altitude is smaller than the estimated uncertainty in the height determination.

3.4. Selection of the Located-Source Data Set

[34] This gain (by a factor of 140/4) shown in Figures 4–7 is one of the higher-gain cases we have encountered in the

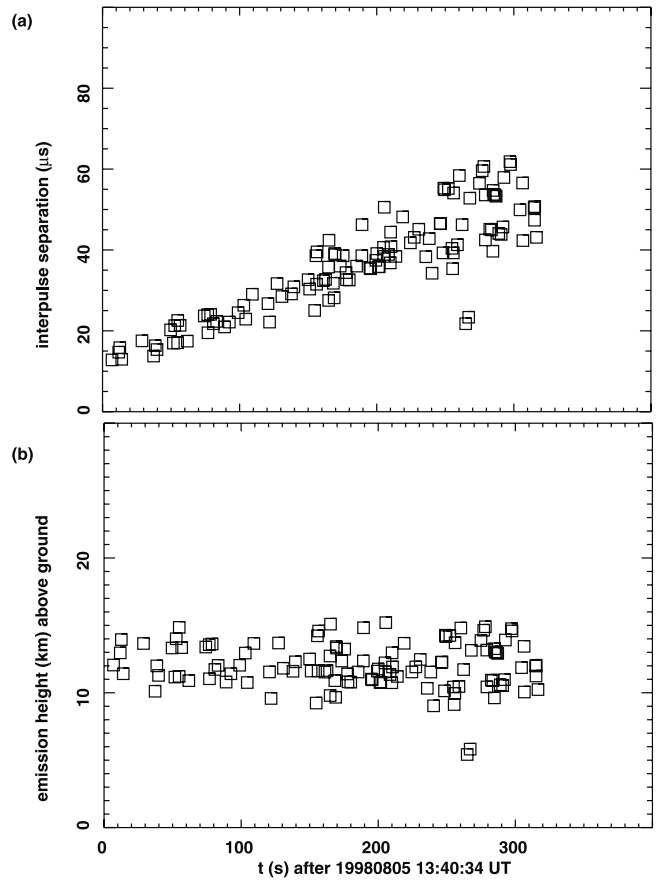

Figure 7. (a) Interpulse separation for each of the IC discharges in Figure 5. (b) Inferred discharge height for each of the IC discharges in Figure 5.

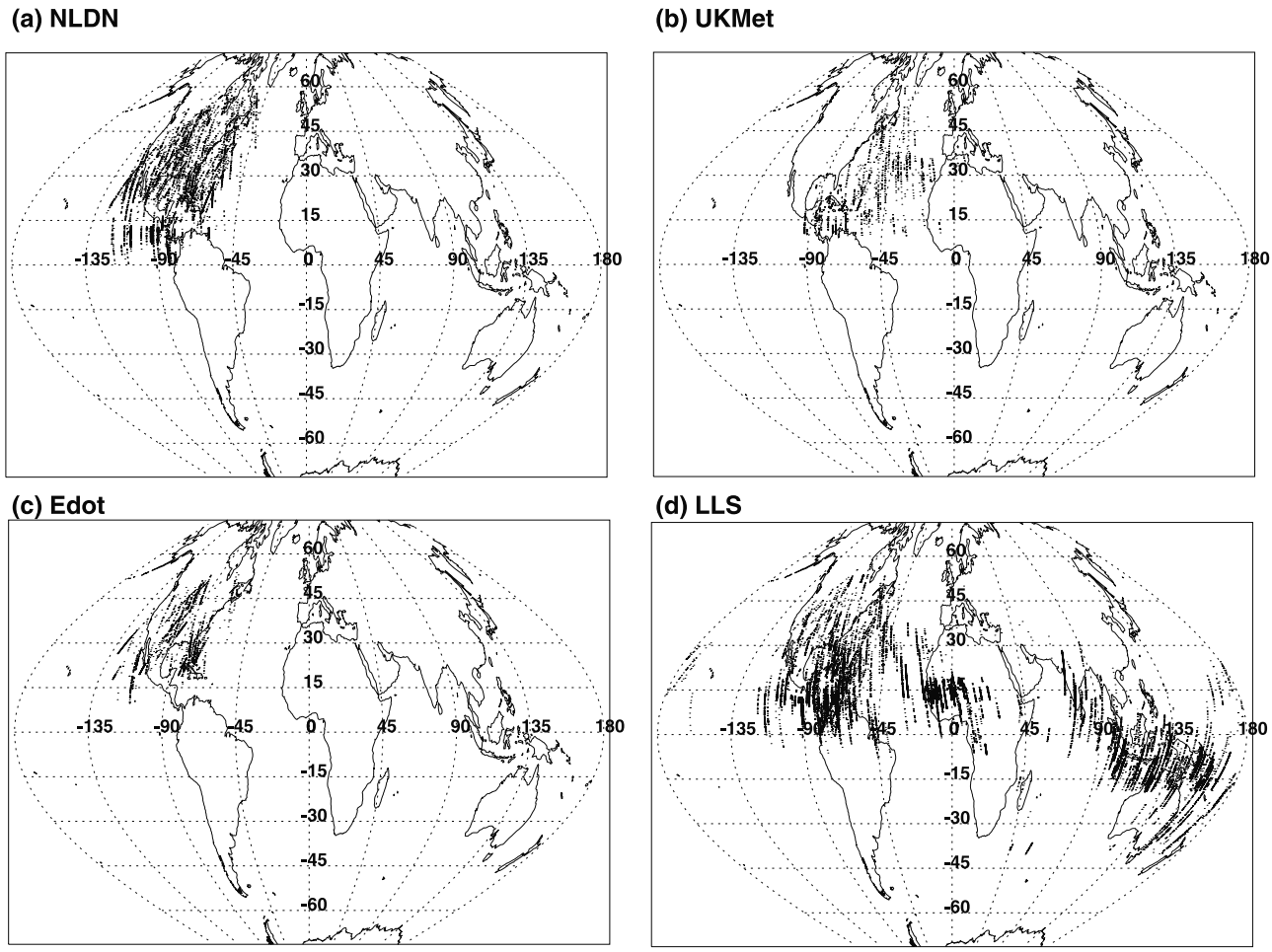

Figure 8. Maps of subsatellite positions for RF recordings for which lightning positions can be borrowed. The breakdown of these 67,578 locations' provenance is: (a) 7,671 from NLDN, (b) 2,828 from the UK Met Office array, (c) 2,236 from the Los Alamos Sferic-Waveform array, and (d) 54,843 from the LLS aboard FORTE.

location-borrowing treatment of FORTE data. Most of the events whose locations are already known do not have clear associations with such well-defined, isolated storms. Also, most of the events whose locations are already known do not occur in at least three located events with less than 300 km of scatter about their mean position. The total number of FORTE RF pulses whose location we can trust because they meet the two stringent criteria, after all borrowing has been done, is 161,554. Of these, we further downselect to high-snr IC pulse pairs, of which there are 67,578. This number excludes all cloud-to-ground phenomena (e.g., the ground-attachment transients described by *Jacobson and Shao* [2002a]) and pulses of intracloud origin that are either too wide (>10 μs) or too weak (<20 X noise) relative to the background radio noise. The first condition (width >10 μs) effectively excludes most recorded recoil-streamer pulses such as shown elsewhere in Figure 2 of *Light et al.* [2001a]. The breakdown of these 67,578 locations' provenance is: 7,671 from NLDN, 2,828 from the UK Met Office array, 2,236 from the Los Alamos Sferic-Waveform array, and 54,843 from the LLS aboard FORTE. Figure 8 shows the subsatellite positions (not the source positions) for events located with the aid of each of those four systems. It is seen that NLDN mainly services FORTE during passes near North America, that the UK Met Office array has provided useful locations for Atlantic maritime regions, that the Los Alamos Sferic-Waveform array ("Edot") has been most useful for North America and in particular the Florida region, and that the LLS has been most useful for low latitudes at all longitudes.

4. Results and Discussion

4.1. Statistics of Discharge Height and Radiated Peak Power

[35] The distribution of discharge heights for the 67,578 selected IC pulses is shown in Figure 9. The distribution falls rapidly above 14 km. This is consistent with the experience of other height-determining systems, for example the Lightning Mapping Array (LMA) [*Rison et al.*, 1999; *Thomas et al.*, 2001]. It is also consistent with the TRMM PR 30-dBz heights associated with cells having LIS-observed lightning [see, e.g, *Toracinta et al.*, 2002, Figure 9]. Finally, it is consistent with the fact that even severe storms are unable to penetrate too far above the convection-capping tropopause. Figure 9 also shows a miniscule number of discharges at or

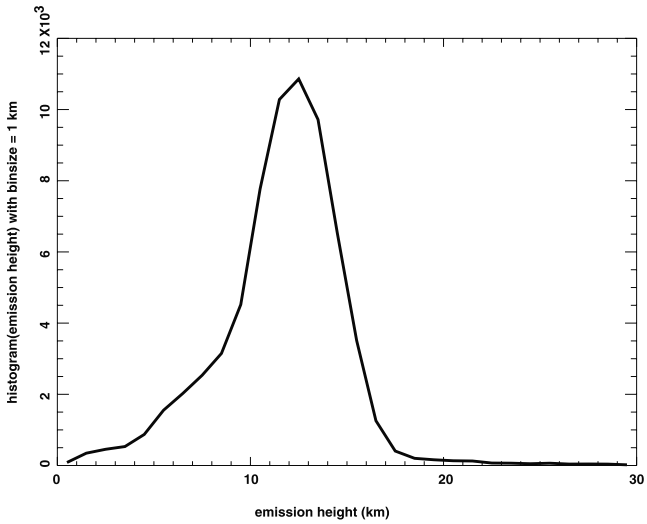

Figure 9. Histogram of discharge height (above reflective ground) for all 67,578 IC discharges for which horizontal positions can be inferred. The binwidth is 1 km, which is comparable to the measurement inaccuracy in determining height.

above 20 km. We cannot say whether those result from spurious location borrowing, or are actually a manifestation of air breakdown associated with "upward lightning" above the cloud top (reviewed by W. A. Lyons et al. (Upward electrical discharges from thunderstorm tops, submitted to *Bulletin of the American Meteorological Society*, 2002)).

[36] The ERP is the peak power in the FORTE low band, which is effectively 26–48 MHz [*Jacobson et al.*, 1999]. The ERP is based on the dechirped [*Jacobson et al.*, 1999] electric field at the satellite, which is then treated to remove the effect of radio carrier noise, squared, averaged over about 1 μs, and converted (knowing the slant distance to the source) to isotropic radiated power. The distribution of the logarithm (base 10) of the at-source ERP for the 67,578 selected IC pulses is shown in Figure 10. The low-power part of the distribution, certainly below 4 kW, is heavily biased by the trigger threshold (see discussion in section 3.2 above.) The high-power end of the distribution, say above 10 kW, is purely due to the intrinsic lightning ERP spectrum and is not distorted by the trigger threshold on FORTE.

[37] The high-power tail of the ERP distribution, certainly above 100 kW and in many cases above only 40 kW, can be triggered upon even from GPS [*Suszcynsky et al.*, 2000a]. This high-power tail is expected to serve as the most useable lightning storm observable for a GPS-borne global monitor. Lightning observations from GPS suffer about a 12-dB worse signal-to-background ratio relative to FORTE, due to the larger viewed disk of the Earth and hence larger contributory area for anthropogenic radio noise.

[38] The IC discharges with ERP > 100 kW also coincide with the intense, incoherent, unpolarized, and relatively wide (3–5 μs) pulses illustrated in Figure 2a. This class of pulses has been shown elsewhere to occur either in temporal isolation or as initiators of IC flashes but never in the midst of a flash [*Jacobson and Light*, 2003]. This class of pulses has also been shown [see, e.g., *Jacobson et al.*, 1999, Figures 18–20] to have a relatively white spectrum in the lower VHF (30–150 MHz). The same class of pulses is seen by the LMA [*Thomas et al.*, 2001] in their passband 60–66 MHz. Scaling by bandwidth, FORTE's ERP > 100 kW for these events would correspond to an LMA ERP >30 kW, which is consistent with the tail seen in the LMA distribution of ERP [see *Thomas et al.*, 2001, Figures 2 and 4].

[39] Another similarity of FORTE with LMA is in the power law behavior of the pulse intensity (E^2 at the satellite) and ERP distributions. Figure 11a shows the pulse-intensity distribution in bins of 10^{-8} $(v/m)^2$, on a log-log scale. The dashed line is tangent to the high-intensity end of the distribution and has a slope of −1.74 (±0.1). The same data yield the ERP distribution in Figure 11b, with a bin size of 1 kW and again with log-log scales. There is a slight change of slope above 20 kW, and the high-ERP wing of the distribution shows a power law (dashed line) of −1.05 (±0.1). *Thomas et al.* [2001] (see their Figures 2–6) note a consistent slope of about −1 on the LMA distributions of ERP on the high-power side of the maximum population density. Thus there is apparent consistency between FORTE and LMA distributions of ERP for IC pulses, although this could be accidental.

[40] Earlier work [see *Light and Jacobson*, 2002, Figure 10] on FORTE had showed that there is a statistical tendency for IC discharges located higher above the ground to have greater ERP. We test that preliminary finding with more data here, using all the 67,578 selected IC pulses for which we have either primary or borrowed locations. Figure 12 shows two-dimensional histograms of $\log_{10}$(ERP) (horizontal axis) and IC discharge height (vertical axis), for IC pulses whose location provenance is (a) NLDN, (b) UK Met, (c) the Los Alamos Sferic-Waveform array ("Edot"), and (d) LLS. The distributions show a noticeable tilt upward, so that there is a weak tendency for ERP to increase while emission height increases. Notice that this is not a relationship between flash rate and storm height; rather, it is

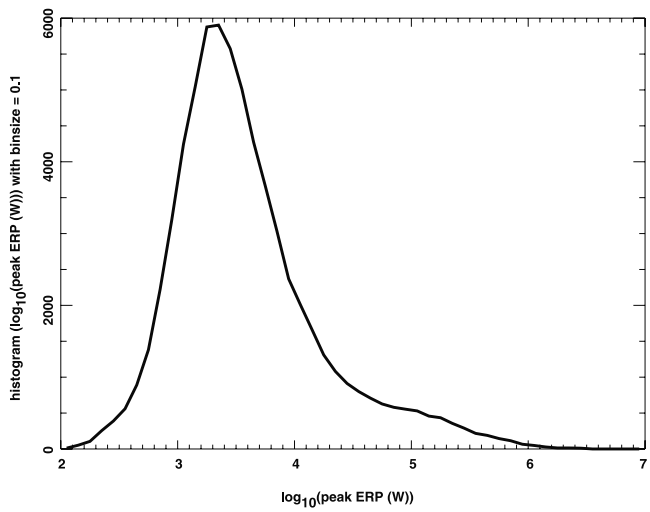

Figure 10. Histogram of the logarithm (base 10) of the ERP (W) for all 67,578 IC discharges for which horizontal positions can be inferred. The binwidth is 0.1 in dimensionless units.

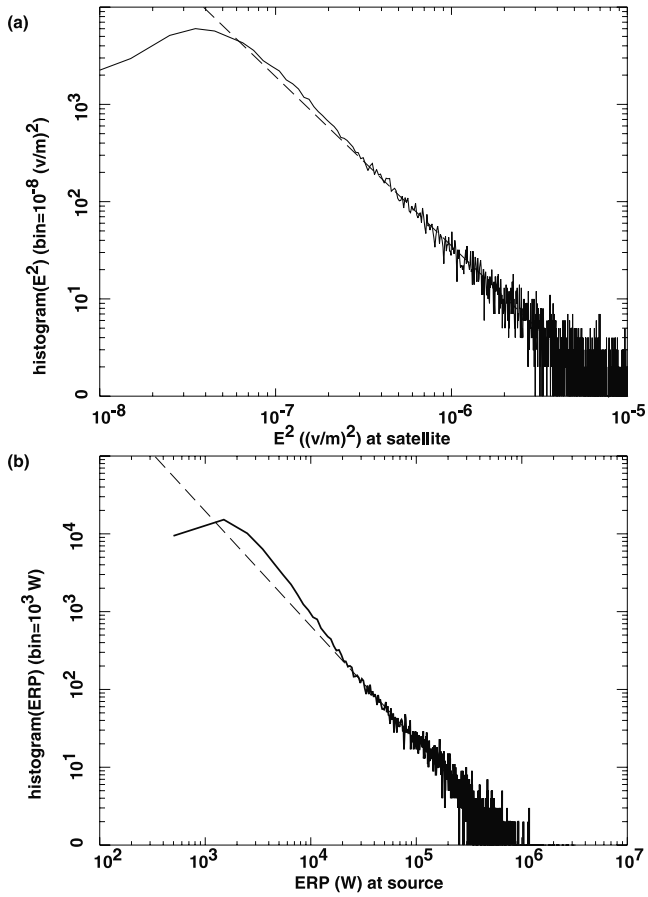

Figure 11. (a) Histogram of E^2 (intensity) at satellite, with binwidth 10^{-8} $(v/m)^2$. Dashed line has log-log slope of -1.74. (b) Histogram of ERP in band 26–48 MHz at source, with binwidth 10^3 W. Dashed line has log-log slope of -1.05. Data include all 67,578 IC discharges for which horizontal location is known.

a (weak) relationship between emitted power (per event) and emission height. The following section replaces this apparent data relationship with one that is slightly less noisy, and more physically motivated.

4.2. Observed Lightning Capping Layer

[41] The observed relationships between OTD or LIS lightning flash rates, on the one hand, and either PR radar heights or microwave-imager temperature ice-scattering signatures, on the other hand, relate lightning vigor to the vertical development of the storm. This is in keeping with cloud-microphysics arguments [e.g., *Baker et al.*, 1999; *Blyth et al.*, 2001] and electrical-generator-scaling arguments (reviewed by *Boccippio* [2002]). Although FORTE flash rates have not yet been corrected for observing biases, and hence cannot be used in the manner that OTD and LIS flash rates have been used, it is nonetheless true that FORTE can measure the ERP of an IC pulse without bias as long as the ERP exceeds some threshold, on the order of 10 kW (see Figure 11, and discussion in section 4.1 above). It would therefore be in keeping with prior practice on optical flash rates, and with model-based physical expectations too, if we attempt to relate the FORTE observations of pulse ERP to the vertical development of the storms in which those pulses are generated. This is different from simply graphing the discharge height versus the discharge ERP as was done in Figure 12 above.

[42] FORTE lacks a downlooking radar and a microwave imager, and thus cannot, unlike TRMM, perform its own direct autonomous measurements of either storm height or storm glaciation. Nonetheless, we can use the swarm of FORTE discharge-height determinations for a given storm as an indicator of the height range through which lightning occurs in that storm, and then identify the top of that height range as the effective top of the electrified storm. In order to do this, we need to consider all data from a given storm observation together, not just individual discharges autonomously.

[43] The example storm of Figures 4–7 (above) suggests how to do this: The swarm of discharge heights (Figure 7b) indicates a capping layer near 14–15 km for the electrified portion of this storm. Since the part of the cloud in which IC discharges occur is generally in the radar-reflectivity core right up to the top of that core [see, e.g., *Thomas et al.*, 2001, Figure 1], our use of discharge peak heights as a proxy for cloud height is of a similar validity as use of radar-reflectivity levels. There is considerable evidence that the upward channels of lightning coincide with the high-radar-cross-section precipitation core of the storm [*Maier et al.*, 1995; *Scott et al.*, 1995]. Thus for the storm of Figures 4–7, the effective storm height would be 14–15 km. That storm's IC discharges show relatively uniform occupancy of height in the range 10–14 km, and the discharges tend not to be clustered into multidischarge flashes. In fact, multi-discharge flashes are more typical in FORTE IC data, as is a capping height that is rather more obvious than in Figure 7b.

[44] Figure 13 shows four typical time series of discharge height for passes by FORTE near storms. Figure 13a shows a pass in which only a rather height-delimited capping layer is observed. When we see such a layer, which is very often, we typically see flashes draping downward but not extending upward, from the capping layer. Figure 13b shows incipient appearance of flashes below the capping layer. Figure 13c shows well-developed, high-multiplicity flashes below the capping layer. Figure 13d shows the less usual case of vertically extensive, high-multiplicity flashes, without an observed capping layer. Following insights provided by the LMA [*Rison et al.*, 1999; *Thomas et al.*, 2001], we assume that the capping layer is the highest laminar positive charge layer, into which negative-breakdown leaders are propagating. It is believed that the individual steps of the negative leaders provide many of the FORTE IC pulses, at least those IC pulses in the weaker, more polarized, and smaller-width category as typified by Figure 2b above [*Jacobson and Light*, 2003]. The highest-ERP pulses, such as in Figure 2a, are usually seen somewhat below the capping positive-charge layer [*Jacobson and Light*, 2003; *Rison et al.*, 1999; *Thomas et al.*, 2001].

[45] In order to impose a uniform and automatically implementable standard, we choose the 90th-percentile height (of all the discharges in any given storm) to serve as the effective storm height. In the majority of storms, which have a clear capping layer that contains many of the storm's observed discharges, the 90th-percentile height is the height of the capping layer. Some of the storms contain

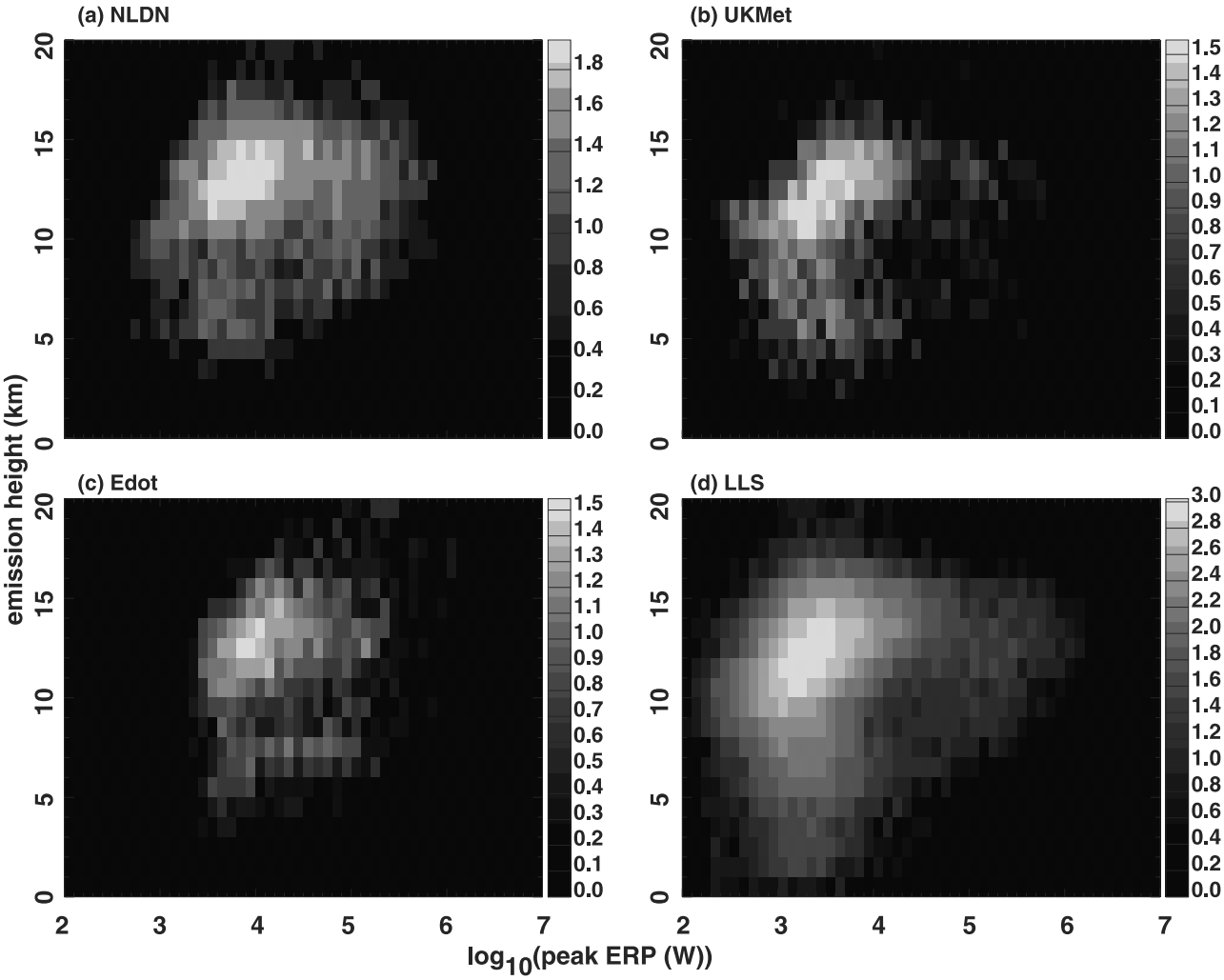

Figure 12. Two-dimensional histograms of logarithm (base 10) of the ERP (W), horizontal axis, and discharge height (km), vertical axis, for all 67,578 IC events as follows: (a) 7,671 from NLDN, (b) 2,828 from the UK Met Office array, (c) 2,236 from the Los Alamos Sferic-Waveform array, and (d) 54,843 from the LLS aboard FORTE.

fewer than 50 IC-discharge events, but we set a threshold of 50 as the minimum number of events in a storm in order for that storm to be considered capable of revealing a statistically meaningful 90th-percentile height. There are 381 storms containing at least 50 IC-discharge events in each storm and having acceptable borrowed locations. Together these 381 storms comprise 53,116 total IC events, or about 80% of the total number (67,578) of IC events in the selected database. Figure 14a shows the distribution of 90th-percentile heights for these 381 storms. There are essentially no such storms with 90th-percentile heights less than 10 km or more than 17 km.

[46] Figure 14b shows the normalized-height distribution of the 53,116 IC events contained in the 381 storms. The normalization for each event is by the 90th-percentile height of the storm containing that event. The small peak at 1.0 (dashed vertical line) is due to the small subset of storms (like the example in Figure 13a above) that have FORTE-recorded events only in the capping layer and nowhere else. The distribution of normalized event height shows that the high-altitude fall-off in event occurrence is much steeper than the low-altitude fall-off. For example, the magnitude of the slope is about three times greater between normalized heights 1.0 and 1.1 than between normalized heights 0.6 and 0.9. This asymmetry between the gradient lengths is due to usual presence (see Figure 13 above) of a capping layer on top, above which there are no, or only very rare, flashes, whereas the many vertically extended flashes that do occur (e.g., Figures 13b and 13c) are always below the capping layer.

[47] The ERP distribution of Figure 10 shows the high-power shoulder (at ERP > 30 kW) that will constitute the useful signature for a lightning monitor amid the greater radio noise experienced at GPS orbit. The question is, is this high-ERP signature merely an idiosyncratic curiosity of shallow (and meteorologically insignificant) storms, or is it instead a tell-tale of deep convection and hence of meteorological settings for severe weather (W2001)? Is there a statistical relationship between ERP and some measure of convective depth (storm height)? Some hints have been seen elsewhere of such a relationship [*Light and Jacobson*, 2002], and our results summarized in Figure 12

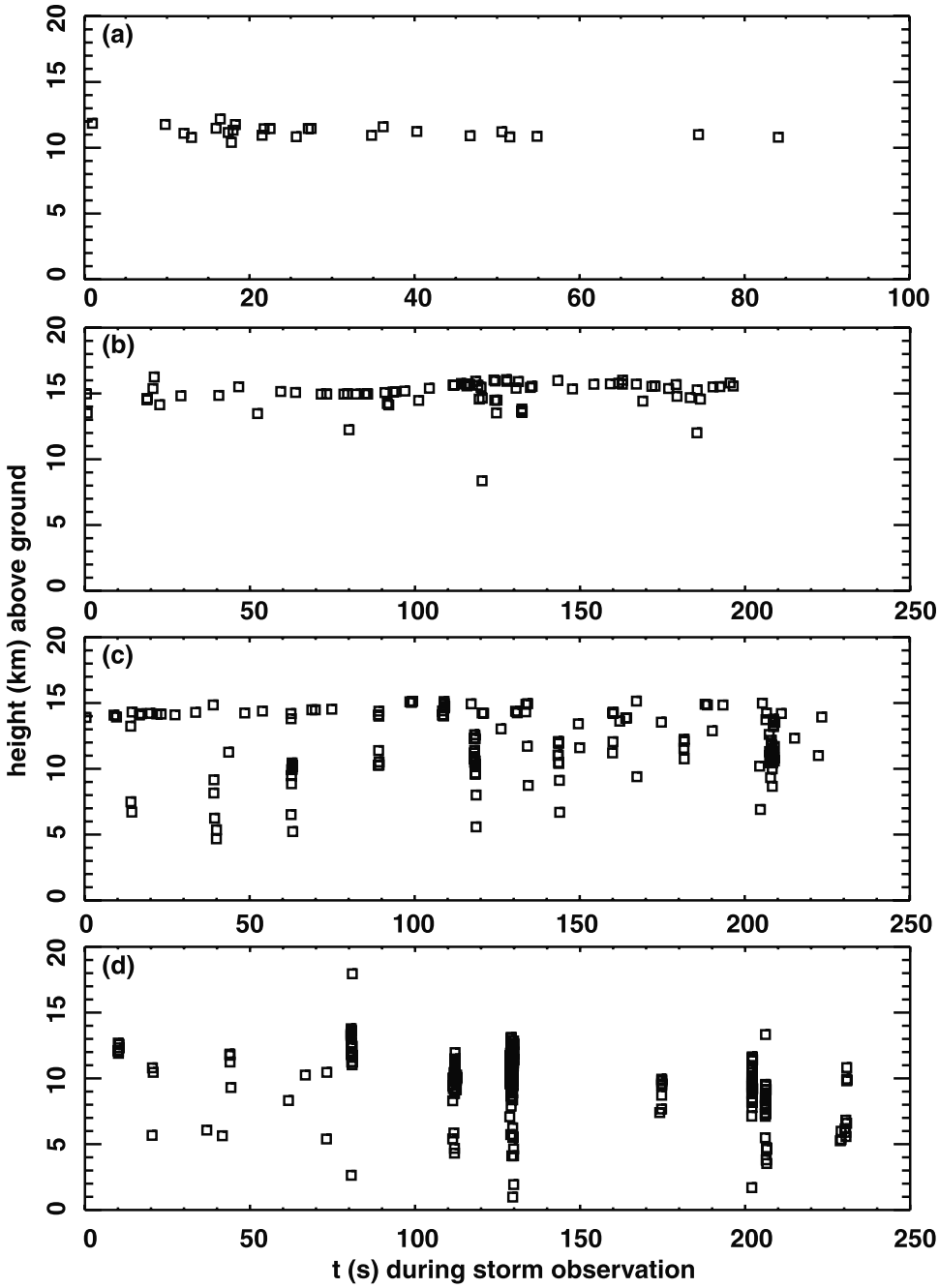

Figure 13. Examples of IC discharge height patterns during time, for FORTE passes in view of four separate storms.

indicate a weak but detectable statistical correlation between ERP and discharge height. Unfortunately, that relationship is partially spoiled by the fact that even where a storm top can get quite high (>14 km), the powerful discharges can occur somewhat lower in the storm [*Jacobson and Light*, 2003; *Rison et al.*, 1999; *Thomas et al.*, 2001], so that the ERP/height relationship is confused.

[48] To study this further, we take all 53,116 total IC events belonging to storms containing at least 50 IC events, and split these into quartiles of discharge height. The ERP distributions for the four quartiles are shown in Figure 15a. The quartiles individually have mean discharge heights (1) 9.8 km, (2) 11.6 km, (3) 13.0 km, and (4) 14.9 km. These are marked in Figure 15a by (1) light solid, (2) light dashed, (3) heavy solid, and (4) light dashed curves. At ERP values below 40 kW, there is a clear statistical relationship between ERP and discharge height: The higher the discharge height, the more displaced to higher ERP is the distribution of ERP. However, at high ERP (>40 kW), a power range at which future GPS monitoring will be performed, the height-to-ERP relationship is muddied: The population with ERP > 40 kW of 9.8-km height discharges exceeds the population of the 11.6-km height and roughly equals the population of the 13.0-km height. That is, there is a nonmonotonic

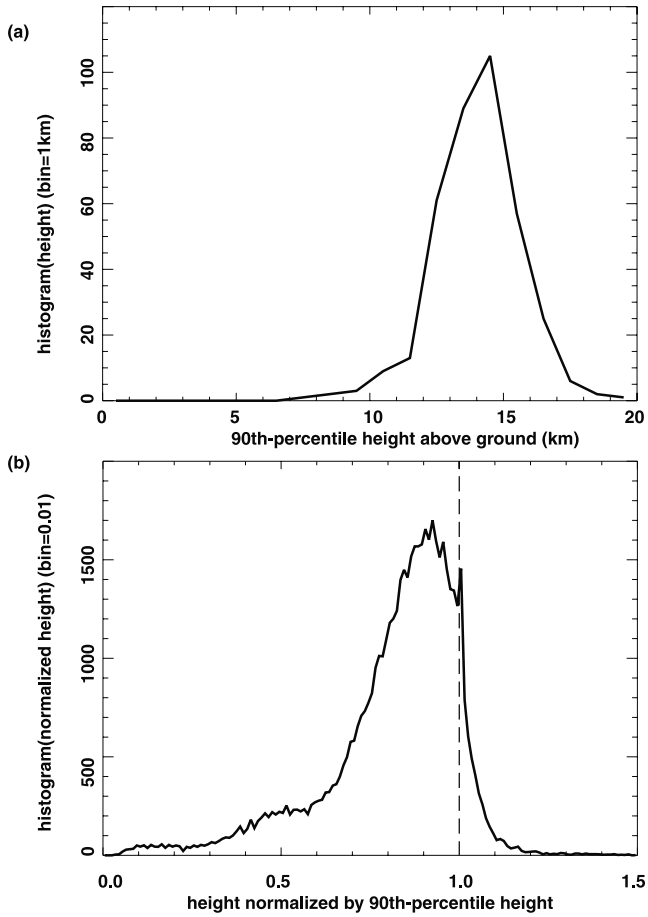

Figure 14. (a) Histogram of 90th-percentile (capping) height for 381 storm passes that contain at least 50 IC discharges. Binwidth is 1 km. (b) Histogram of heights of all 53,116 IC discharges from those storms, normalized by the 90th percentile height of the parent storm. Binwidth is 0.1.

relationship of height to ERP above 40 kW, precisely in the power range that will be useful for monitoring lightning from GPS. This is due to the tendency of the most powerful IC discharges to occur somewhat below the capping layer rather than at the capping layer [*Jacobson and Light*, 2003; *Rison et al.*, 1999; *Thomas et al.*, 2001].

[49] Figure 15b is similar to Figure 15a but groups the same 53,116 IC pulses into quartiles of capping height (90th-percentile height) of each discharge's parent storm. These capping height quartiles have average capping heights of (1) 12.2 km, (2) 13.8 km, (3) 14.6 km, and (4) 15.9 km. Organized in this manner, it is clear that the high-ERP IC discharges are more likely to occur for storms with the highest capping heights. For example, for ERP > 40 kW, the observed likelihood of IC discharges is ~10 times greater for storms with capping height in the 15.9-km class than for storms with capping height in the 12.2-km class. We reiterate that these high-ERP events are precisely the events that can be seen against background noise at GPS orbit [*Suszcynsky et al.*, 2000a]. Thus we conclude from Figure 15b that the very-powerful discharges (ERP > 40 kW in the passband 26–48 MHz) in the FORTE database, and on which a future GPS lightning monitor can be expected to rely, are heavily selective for very deep convection.

5. Summary and Discussion

[50] This paper has presented distributions of both the ERP (in a 26–48 MHz passband) and discharge height for the entire database of IC discharges which (a) are recorded by FORTE and (b) have horizontal locations borrowed from other systems. We have shown that, below several kW, the ERP distribution is artificially truncated by FORTE trigger-thresholds that vary geographically. On the other hand, we have shown that the ERP distributions above 10 kW are sufficiently above the trigger thresholds that the distribution is sampled without bias.

[51] The relationship between individual discharge height and ERP is suggestive but somewhat muddied by the fact that the powerful discharges (ERP > 40 kW) often occur

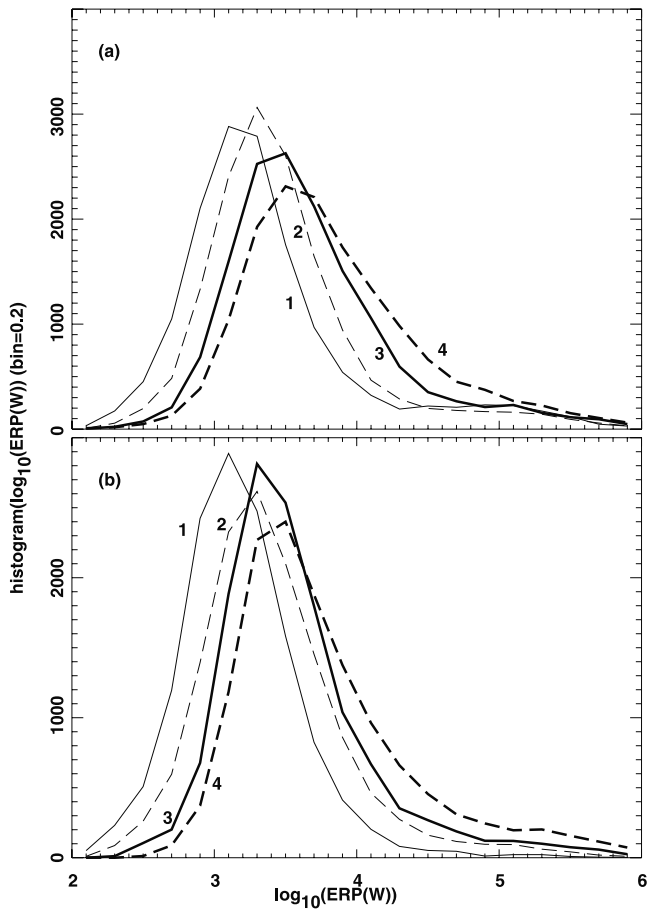

Figure 15. Histograms of logarithm (base 10) of the ERP (W) with binwidth 0.2, for all 53,116 total IC events belonging to storms containing at least 50 IC events. (a) Divided into quartiles of discharge height. The quartiles individually have mean discharge heights (1) 9.8 km, (2) 11.6 km, (3) 13.0 km, and (4) 14.9 km. (b) Divided into quartiles of 90th-percentile height (capping height) of the parent storm. The quartiles individually have mean 90th-percentile heights of (1) 12.2 km, (2) 13.8 km, (3) 14.6 km, and (4) 15.9 km.

below the capping layer of electrical breakdown. We have shown how there is a clearer relationship between, on the one hand, occurrence of discharges with ERP > 40 kW, and, on the other hand, the capping height of the storm containing the discharges. Moreover, this relationship is quite sharply defined: For ERP > 40 kW, the observed likelihood of IC discharges is ~ten times greater for storms with capping height in the 15.9-km class than for storms with capping height in the 12.2-km class. This implies that triggering on RF emissions with ERP > 40 kW is strongly selective for the deepest convection.

[52] Lightning's strong selectivity for deep convection appears to be a recurrent theme in lightning observations. The present result with FORTE simply adds a more extreme form of selectivity imposed when we require ERP > 40 kW in the 22–48 MHz passband. The original hypothesis in this field, that the flash rate varies as the fifth power of the cloud top height, was by itself based on observational evidence of strong selection for deep convection (see W2001 and updated observations of *Boccippio* [2002] and *Ushio et al.* [2001]). The remarkable correlations between continental lightning seen with LIS, and cloud-ice microwave scattering seen with TMI [*Toracinta et al.*, 2002], again indicate a strongly nonlinear enhancement in the lightning activity of a storm, if that storm has unusually deep vertical development. This indicates a common outcome of earlier studies and the FORTE results reported here. However, whereas essentially all previous measures of lightning vigor have used flash rate, the present result with FORTE pertains to lightning emission power. We intend to perform a bias-corrected FORTE flash-rate survey in the near future. At that time, we will be able to examine the dependence of FORTE-observed flash rates on storm characteristics, including storm height.

[53] **Acknowledgments.** This work was performed under the auspices of the U.S. Department of Energy.

References

Baker, M. B., A. M. Blyth, H. J. Christian, J. Latham, K. L. Miller, and A. M. Gadian, Relationship between lightning activity and various thundercloud parameters: Satellite and modelling studies, *Atmos. Res.*, *51*, 221–236, 1999.

Blyth, A. M., H. J. J. Christian, K. Driscoll, A. M. Gadian, and J. Latham, Determination of ice precipitation rates and thunderstorm anvil ice contents from satellite observations of lightning, *Atmos. Res.*, *59–60*, 217–229, 2001.

Boccippio, D. J., Lightning scaling relations revisited, *J. Atmos. Sci.*, *59*, 1086–1104, 2002.

Boccippio, D. J., K. Driscoll, W. Koshak, R. Blakeslee, W. Boeck, D. Buechler, H. Christian, and S. Goodman, The Optical Transient Detector (OTD): Instrument characteristics and cross-sensor validation, *J. Atmos. Oceanic Technol.*, *17*, 441–458, 2000a.

Boccippio, D. J., S. J. Goodman, and S. Heckman, Regional differences in tropical lightning distributions, *J. Appl. Meteorol.*, *39*, 2231–2248, 2000b.

Boccippio, D. J., S. Heckman, and S. J. Goodman, A diagnostic analysis of the Kennedy Space Center LDAR network: 1. Data characteristics, *J. Geophys. Res.*, *106*, 4769–4786, 2000c.

Boccippio, D. J., S. Heckman, and S. J. Goodman, A diagnostic analysis of the Kennedy Space Center LDAR network: 2. Cross-sensor studies, *J. Geophys. Res.*, *106*, 4787–4796, 2000d.

Boccippio, D. J., K. L. Cummins, H. J. Christian, and S. J. Goodman, Combined satellite- and surface-based estimation of the intracloud-cloud-to-ground lightning ratio over the continental United States, *Mon. Weather Rev.*, *129*, 108–122, 2001.

Christian, H. J., R. J. Blakeslee, and S. J. Goodman, The detection of lightning from geostationary orbit, *J. Geophys. Res.*, *94*, 13,329–13,337, 1989.

Christian, H. J., et al., Global frequency and distribution of lightning as observed by the Optical Transient Detector (OTD), in *11th International Conference on Atmospheric Electricity*, edited by H. Christian, pp. 726–729, Global Hydrol. and Clim. Cent., NASA Marshall Space Flight Cent., Huntsville, Ala., 1999a.

Christian, H. J., et al., The Lightning Imaging Sensor, in *11th International Conference on Atmospheric Electricity*, edited by H. Christian, pp. 746–749, Global Hydrol. and Clim. Cent., NASA Marshall Space Flight Cent., Huntsville, Ala., 1999b.

Jacobson, A. R., and T. E. L. Light, Bimodal radiofrequency pulse distribution of intracloud-lightning signals recorded by the FORTE satellite, *J. Geophys. Res.*, *108*, doi:10.1029/2002JD002613, in press, 2003.

Jacobson, A. R., and X.-M. Shao, Using geomagnetic birefringence to locate sources of impulsive, terrestrial VHF signals detected by satellites on orbit, *Radio Sci.*, *36*(4), 671–680, 2001.

Jacobson, A. R., and X.-M. Shao, FORTE satellite observations of very narrow radiofrequency pulses associated with the initiation of negative cloud-to-ground lightning strokes, *J. Geophys. Res.*, *107*(D22), 4661, doi:10.1029/2001JD001542, 2002a.

Jacobson, A. R., and X.-M. Shao, On-orbit direction-finding of lightning radio-frequency emissions recorded by the FORTE satellite, *Radio Sci.*, *37*(4), 1064, doi:10.1029/2001RS002510, 2002b.

Jacobson, A. R., S. O. Knox, R. Franz, and D. C. Enemark, FORTE observations of lightning radio-frequency signatures: Capabilities and basic results, *Radio Sci.*, *34*(2), 337–354, 1999.

Jacobson, A. R., K. L. Cummins, M. Carter, P. Klingner, D. Roussel-Dupré, and S. O. Knox, FORTE radio-frequency observations of lightning strokes detected by the National Lightning Detection Network, *J. Geophys. Res.*, *105*, 15,653–15,662, 2000.

Kirkland, M. W., D. M. Suszcynsky, J. L. L. Guillen, and J. L. Green, Observations of terrestrial lightning at optical wavelengths by the FORTE satellite photodiode detector, *J. Geophys. Res.*, *106*, 33,499–33,509, 2001.

Koshak, W. J., R. J. Solakiewicz, D. D. Phanord, and R. J. Blakeslee, Diffusion model for lightning radiative transfer, *J. Geophys. Res.*, *99*, 14,361–14,371, 1994.

Kummerow, C., W. Barnes, T. Kozu, J. Shiue, and J. Simpson, The Tropical Rainfall Measuring Mission (TRMM) sensor package, *J. Atmos. Oceanic Technol.*, *15*, 809–817, 1998.

Lee, A. C. L., An operational system for the remote location of lightning flashes using a VLF arrival time difference technique, *J. Atmos. Oceanic Technol.*, *3*, 630–642, 1986.

Light, T. E. L., and A. R. Jacobson, Characteristics of impulsive VHF lightning observed by the FORTE satellite, *J. Geophys. Res.*, *107*(D24), 4756, doi:10.1029/2001JD001585, 2002.

Light, T. E., D. M. Suszcynsky, and A. R. Jacobson, Coincident radio frequency and optical emissions from lightning, observed with the FORTE satellite, *J. Geophys. Res.*, *106*, 28,223–28,231, 2001a.

Light, T. E., D. M. Suszcynsky, M. W. Kirkland, and A. R. Jacobson, Simulations of lightning optical waveforms as seen through clouds by satellites, *J. Geophys. Res.*, *106*, 17,103–17,114, 2001b.

Maier, L., C. Lennon, P. Krehbiel, M. Stanley, and M. Robison, Comparison of lightning and radar observations from the KSC LDAR and NEXRAD radar systems, in *27th Conference on Radar Meteorology*, pp. 648–650, American Meteorol. Soc., Boston, Mass., 1995.

Massey, R. S., S. O. Knox, R. C. Franz, D. N. Holden, and C. T. Rhodes, Measurements of transionospheric radio propagation parameters using the FORTE satellite, *Radio Sci.*, *33*(6), 1739–1753, 1998.

Rison, W., R. J. Thomas, P. R. Krehbiel, T. Hamlin, and J. Harlin, A GPS-based three-dimensional lightning mapping system: Initial observations in central New Mexico, *Geophys. Res. Lett.*, *26*, 3573–3576, 1999.

Scott, R., P. Krehbiel, M. Stanley, and S. McCrary, Relation of lightning channels to storm structure from interferometer and dual-polarization radar observations, in *27th Conference on Radar Meteorology*, pp. 645–647, Am. Meteorol. Soc., Boston, Mass., 1995.

Shao, X.-M., and A. R. Jacobson, Polarization observations of broadband VHF signals by the FORTE satellite, *Radio Sci.*, *36*(6), 1573–1589, 2001.

Shao, X.-M., and A. R. Jacobson, Polarization observations of lightning-produced VHF emissions by the FORTE satellite, *J. Geophys. Res.*, *107*(D20), 4430, doi:10.1029/2001JD001018, 2002.

Smith, D. A., K. B. Eack, J. Harlin, M. J. Heavner, A. R. Jacobson, R. S. Massey, X. M. Shao, and K. C. Wiens, The Los Alamos sferic array: Ground truth for the FORTE satellite, *J. Geophys. Res.*, *107*(D13), 4183, 10.1029/2001JD000502, 2001.

Suszcynsky, D., A. Jacobson, J. Fitzgerald, C. Rhodes, E. Tech, and D. Roussel-Dupre, Satellite-based global lightning and severe storm monitoring using VHF receivers, *Eos Trans. AGU*, *81*(48), Fall Meet. Suppl., F91, 2000a.

Suszcynsky, D. M., M. W. Kirkland, A. R. Jacobson, R. C. Franz, S. O. Knox, J. L. L. Guillen, and J. L. Green, FORTE observations of simulta-

neous VHF and optical emissions from ligthning: Basic phenomenology, *J. Geophys. Res.*, *105*, 2191–2201, 2000b.

Suszcynsky, D. M., T. E. Light, S. Davis, M. W. Kirkland, J. L. Green, and J. Guillen, Coordinated observations of optical lightning from space using the FORTE photodiode detector and CCD imager, *J. Geophys. Res.*, *106*, 17,897–17,906, 2001.

Thomas, R. J., P. R. Krehbiel, W. Rison, T. Hamlin, J. Harlin, and D. Shown, Observations of VHF source powers radiated by lightning, *Geophys. Res. Lett.*, *28*(1), 143–146, 2001.

Tierney, H., A. R. Jacobson, W. H. Beasley, and P. E. Argo, Determination of source thunderstorms for VHF emissions observed by the FORTE satellite, *Radio Sci.*, *36*(1), 79–96, 2001.

Toracinta, E. R., and E. Zipser, Lightning and SSM/I-ice-scattering mesoscale convective systems in the global tropics, *J. Appl. Meteorol.*, *40*, 983–1002, 2001.

Toracinta, E. R., D. J. Cecil, E. J. Zipser, and S. W. Nesbitt, Radar, passive microwave, and lightning characteristics of precipitating systems in the tropics, *Mon. Weather Rev.*, *130*, 802–824, 2002.

Ushio, T., S. J. Heckman, D. J. Boccippio, H. J. Christian, and Z.-I. Kawasaki, A survey of thunderstorm flash rates compared to cloud top height using TRMM satellite data, *J. Geophys. Res.*, *106*, 24,089–24,095, 2001.

Williams, E. R., The electrification of severe storms, in *Severe Convective Storms*, edited by C. A. I. Doswell, chap. 13, pp. 527–561, Am. Meteorol. Soc., Boston, Mass., 2001.

A. R. Jacobson, Space and Atmospheric Sciences Group, Mail Stop D466, Los Alamos National Laboratory, Los Alamos, NM 87545, USA. (ajacobson@lanl.gov)